Residual strain in the Nb_3Sn 11 T dipole magnet coils for HL-LHC

C. Scheuerlein[1], M. Di Michiel[2], M. Hofmann[3], M. Lorentzon[1], F. Lackner[1], R. Flükiger[1], F. Savary[1], L. Bottura[1]

[1] European Organization for Nuclear Research (CERN), CH 1211 Geneva 23, Switzerland
[2] European Synchrotron Radiation Facility, 6 rue Jules Horowitz, F-38000 Grenoble, France
[3] Forschungsneutronenquelle Heinz Maier-Leibnitz (FRM II), TU München, D-85748 Garching, Germany

Abstract. Nb_3Sn magnets are presently build for the HL-LHC accelerator upgrade and are developed for the Future Circular Collider (FCC) study. The knowledge of the Nb_3Sn strain state distribution in these magnets is required in order to predict their ultimate performance limit. We have measured the Nb_3Sn residual strain distribution in an 11 T dipole accelerator magnet coil. Ambient temperature Nb_3Sn strain maps across 11 T dipole coil cross sections were acquired by means of fast high energy synchrotron X-ray diffraction. Using complementary neutron diffraction measurements the Nb_3Sn residual strain and stress was measured in the four largest conductor blocks of a massive 11 T dipole coil segment.

1. Introduction

The next generation superconducting accelerator magnets [1] presently built for the LHC High Luminosity upgrade (HL-LHC) [2], and developed for the Future Circular Collider (FCC) project, is based on Nb_3Sn superconductors. The superconducting properties of Nb_3Sn are strain sensitive, and the reversible strain dependence of the critical current density (J_c) is commonly ascribed to elastic Nb_3Sn lattice distortions [3,4,5]. When the externally applied load to the coil exceeds a critical value, crack formation in the Nb_3Sn filaments causes an irreversible J_c degradation [6]. Thus, a precise knowledge of the Nb_3Sn strain and stress state in the conductor is required in order to predict the ultimate Nb_3Sn performance limit in magnets and the critical stress levels not to be exceeded during magnet assembly and operation.

The Nb_3Sn strain state in a magnet coil may be influenced by mechanical material properties of the conductor constituents, by friction coefficients between different materials pairs, by cabling, coil winding and Nb_3Sn reaction processes, by the collaring and magnet assembly at ambient temperature and finally by thermal and powering cycles of the magnets during operation.

The first Nb_3Sn lattice spacing measurements reported have been performed using 8.04 keV Cu K_α X-rays provided by commonly used laboratory diffractometers. Since their penetration depth is not sufficient to reach the Nb_3Sn filaments in the wire matrix the measurements were performed either on thin tapes or on wires where the outer sheath was removed [7,8].

Modern high energy synchrotron beamlines provide a very high flux of X-rays with energies >100 keV, exceeding the neutron flux of the most powerful neutron sources by several orders of magnitude. This enables the acquisition of diffraction patterns of Nb_3Sn wires with excellent signal to noise ratio within seconds [9]. This makes high energy synchrotron X-ray diffraction an excellent tool for *in situ* monitoring of the variations of the strain state in composite superconductors submitted to mechanical loads [10], and it enables the acquisition of strain maps with high spatial resolution.

The penetration depth of high energy photons in the highly absorbing metallic Nb_3Sn superconductors is limited to a few millimeters. Neutron diffraction measurements have also been applied to study the strain state in Nb_3Sn wires [11], and they are particularly well suited to study samples with relatively large sample volume, like the ITER Nb_3Sn central solenoid cable [12].

In this article we report for the first time a direct observation of the residual strain distribution in a reacted Nb_3Sn magnet coil, based on high energy synchrotron X-ray diffraction and neutron diffraction measurements.

2. Experimental

2.1 The 11 T dipole Nb_3Sn coil samples

The 11 T dipole [13] magnet coils are wound from unreacted Nb_3Sn Rutherford cables [14,15] consisting of RRP type wires [16], a 25 µm-thick stainless steel core, and a 0.15 mm-thick cable insulation made of a Mica tape and S2/E-glass fiber. After the Nb_3Sn reaction heat treatment with a peak temperature of typically 650 °C, the void space in the reacted coils is filled with epoxy resin CTD-101K from Composite Technology Development [17], in order to improve the electromechanical coil properties.

2.2 High energy synchrotron X-ray diffraction

Synchrotron X-ray diffraction measurements were carried out at the new ID15A High Energy Scattering Beamline of the European Synchrotron (ESRF) in transmission geometry (Figure 1(a)) using a 150 keV monochromatic X-ray beam with a bandwidth of ±300 eV. The X-ray beam had a cross section of 0.2 mm × 0.2 mm. Diffracted X-rays were recorded on a Pilatus3 X CdTe 2M detector, with a sample to detector distance of 1963.6 mm. For the calibration of the photon energy and the sample to detector distance a Cerium Dioxide (CeO_2) reference powder has been used. The samples consist of 3 mm thick coil slices extracted from the Nb_3Sn 11 T dipole coil #107 that previously had been cold tested in a short model magnet. The calculated transmissions of 150 keV photons through a 3 mm thick layer of Nb_3Sn and Cu are 23% and 55%, respectively. For strain mapping, slices have been cut in the center of the straight coil part and in the coil pole end. Figure 1(b) shows a slice from the straight coil part mounted on the goniometer of the ID15A sample stage.

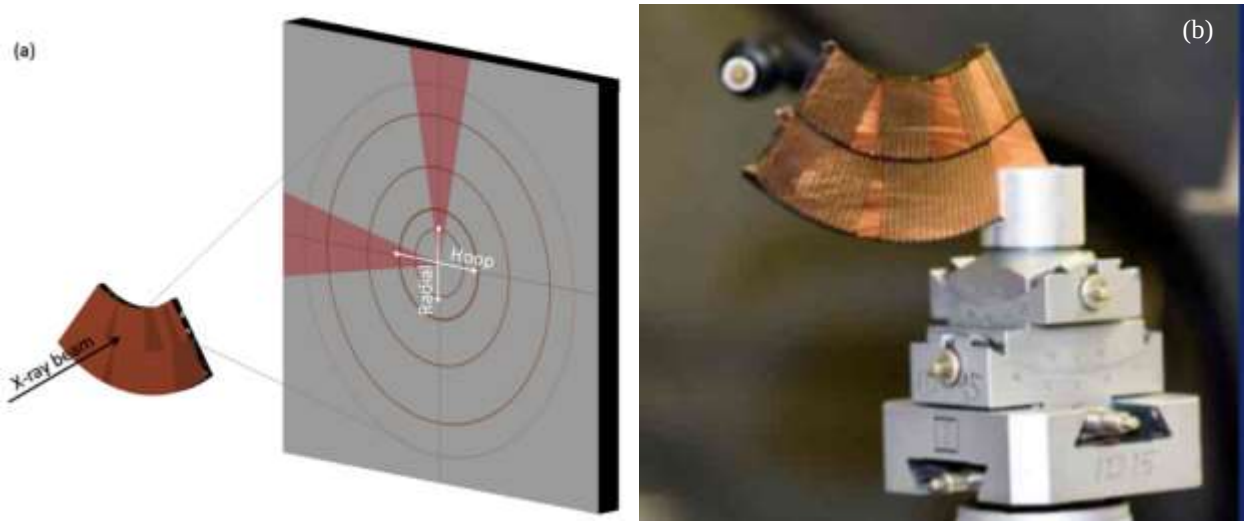

Figure 1: (a) Sketch of ID15A test configuration. (b) 11 T coil slice on the goniometer of the ID15A sample stage.

Entire diffraction rings were recorded in such a way that a d-spacing range from 1.40 to 2.65 Å could be analyzed. The two-dimensional diffraction patterns were caked in 36 circular sectors, each one of them being radially integrated in order to measure lattice parameters from the crystalline planes oriented both in the radial and the hoop direction.

The sample was aligned parallel to the X-ray beam (Ω = 90º) and centered on the rotation axis. In order to achieve a strain resolution of ~0.01% the sample-detector distance needs to be controlled within ~200 µm. During the experiment the wires in the 3 mm thick coil slice were not aligned parallel to the beam, but were tilted by the cable transposition pitch (about 0.45 mm over the 3 mm coil segment thickness). Since this wire tilt affects the wire position where the 200 × 200 µm^2 beam interacts the sample-to-detector distance varies across the 3 mm-thick coil segment. In order to get sufficiently accurate absolute strain results, diffraction scans across the same sample were always acquired two times, at Ω = 0 º and at Ω = 180º. Absolute d-spacing values were obtained by overlaying and averaging the Ω = 0 º and Ω = 180º data points. This procedure also eliminates uncertainties due to small sample bending or thickness variations. The strain resolution of the experiment is better than 0.01% (equivalent to 0.1 detector pixels).

About 100'000 diffractograms were acquired for the strain mapping in the two coil cross sections presented in this article. Single Nb_3Sn (321) and Cu (200) peaks have been fitted with Pseudo Voigt functions and peak position (d-spacing), peak area and peak width were determined from these fits. Multiple peak fitting has been performed on selected diffractograms. The main Nb (100) peak is not present in this configuration (beam parallel to wire drawing axis) because of the strong Nb texture [18].

2.3 Neutron diffraction

Neutron diffraction experiments were performed at the Stress-Spec diffractometer at the FRM II neutron source of the Heinz Maier-Leibnitz Zentrum MLZ [19]. Because of the comparatively deep penetration of the neutron beam, diffraction measurements could be performed in the center of a massive 4 cm-thick 11 T coil #107 segment, and the Nb_3Sn lattice parameter was measured in the center of the four largest conductor blocks in axial, radial and hoop directions (Figure 2).

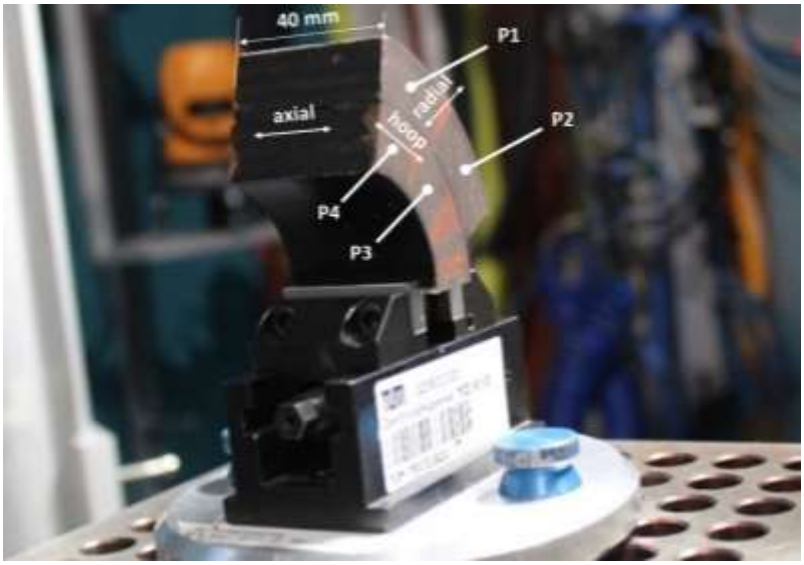

Figure 2: 4 cm-long segment of 11 T short model coil #107 mounted on the Stress-Spec sample stage in axial test configuration. The gauge volume centre positions in radial and hoop position are labelled.

A bent Si (400) monochromator provides a neutron beam with a wavelength of λ=1.672 ±0.003 Å as determined by refinement of the diffractogram of a Si standard powder with FullProf software. The refinement also revealed a 2Θ offset: + 0.232°. The nominal gauge volume 5×5×5 mm^3 is defined by a 5×5 mm^2 slit that shape the beam and by a radial collimator in front of the detector.

A 2Θ range $70.5° < 2\Theta < 83.5°$ was recorded, and Nb_3Sn (321) and Cu (220) reflections were fitted by Gaussian functions. Prior to peak fitting the diffratcograms were corrected for the detector efficiency using incoherent scattering from a Vanadium scan. The acquisition time for one diffractogram in radial and axial directions was 1 hour and in hoop direction 3 hours, respectively.

For measurements at <10 K the sample was mounted on the cold head of a Cryocooler Sumitomo SRDK 101D with a M6 threaded rod. The temperature regulation was performed using a Cernox temperature sensor connected to the cryocooler cold head. The sample temperature was measured with a Cernox sensor screwed to the opposed sample surface.

3. Results

3.1 Nb_3Sn and Cu lattice parameters in extracted wires

In order to measure the Nb_3Sn and Cu lattice parameters at room temperature (RT) without stress exerted by the surrounding coil, individual wires were extracted from coil #107. For the acquisition of the XRD pattern the synchrotron beam was perpendicular to the axis of a single wire that was spinning during data acquisition. The axial and transverse lattice parameters were obtained after caking the diffraction pattern as described above. The texturing of Nb, Cu and Nb_3Sn causes strong differences in the peak intensities in the axial and transverse XRD diffraction pattern shown in Figure 3(a).

For the Stress-Spec measurement a bundle of 20 wires was inserted into a Vanadium tube, the beam being perpendicular to the wire axis. The neutron and X-ray transversal diffractograms of the extracted Nb_3Sn wires are compared in Figure 3(b). In the d-spacing range that was acquired by neutron diffraction four peaks can be identified by comparison with the reference patterns, notably Cu (220), Nb_3Sn (400), Nb (211) and Nb_3Sn (321). The peak beside the bronze (Cu-Sn) (220) reflection is a $\lambda/2$ contribution from Cu (111).

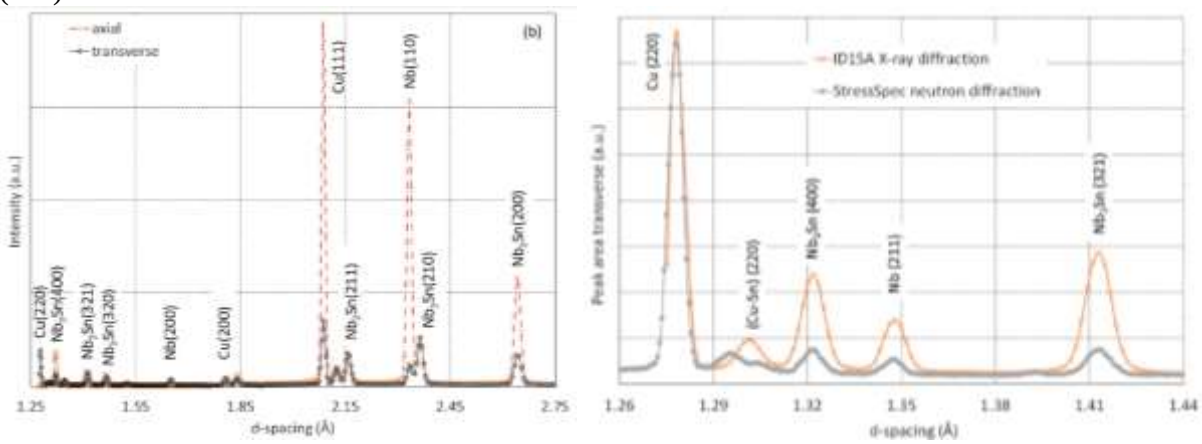

Figure 3: (a) Comparison of single wire axial and transverse XRD pattern. (b) Comparison of XRD and neutron diffraction pattern in transverse direction.

The lattice parameters calculated from the d-spacing of the different reflections measured with ID15A and Stress-Spec are compared in Table 1. Stress-Spec is a strain scanner used for measuring relative diffraction angle variations, rather than for absolute lattice parameter measurements, and the transversal Nb_3Sn (321), Nb (211), Nb_3Sn (400) and Cu (220) lattice parameters obtained with the Stress-Spec diffractometer are shown here for comparison.

Table 1: Comparison of the Nb_3Sn, Nb and Cu lattice parameters calculated from the ID15A and Stress-Spec diffractograms.

	Cu (220)	Cu (111)	Cu (200)	Nb_3Sn (320)	Nb_3Sn (321)	Nb_3Sn (400)	Nb (110)	Nb (211)
ID15A a-axial	n.m.	3.6159	3.6165	5.2865	5.2865	5.2860	3.2993	no peak
ID15A a-trans.	3.6162	3.6156	3.6159	5.2869	5.2865	5.2864	3.3042	3.3012
Stress-Spec a-trans.	3.6147	n.m.	n.m.	n.m.	5.2865	5.2864	n.m.	3.3000

Averaging ID15A lattice parameters calculated for the different reflections one obtains $a_{Cu\text{-}axial}$ = 3.6162 Å, $a_{Cu\text{-}transverse}$ = 3.6159 Å, $a_{Nb3Sn\text{-}axial}$ = 5.2863 Å, and $a_{Nb3Sn\text{-}transverse}$ = 5.2866 Å. This suggests

that Cu in the extracted wire might be under slight axial tension (0.005%) and Nb_3Sn under slight axial pre-compression (0.003%).

Nb residual strain and stress cannot be calculated, the reflections of the strongly textured Nb being not detected in all directions. The comparison between axial and transverse Nb lattice parameters suggests that inside the wire the very thin Nb barriers are under axial pre-compression.

3.2 Nb_3Sn lattice parameter distribution in hoop and radial directions

A photograph of the 3 mm thick coil slice extracted from the 11 T dipole coil center is shown in Figure 4(a). The Nb_3Sn (321) diffraction peak intensity scan obtained for the same slice is shown in Figure 4(b).

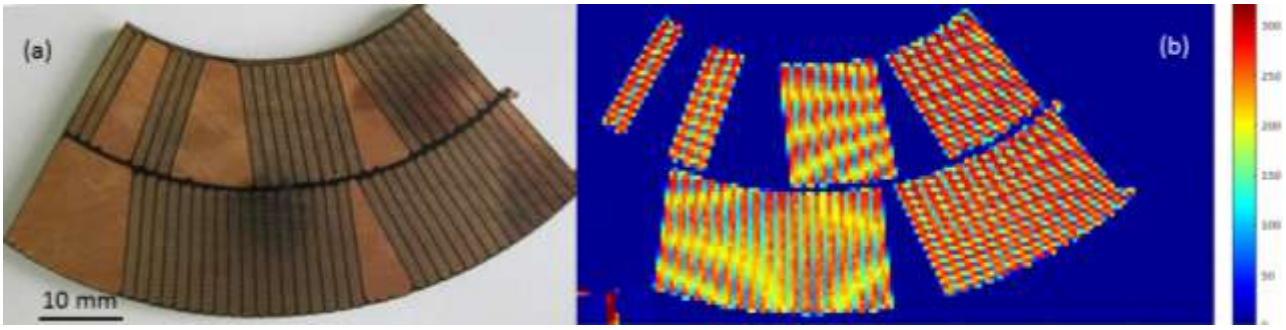

Figure 4: (a) Photograph of the Nb_3Sn 11 T dipole coil. (b) Nb_3Sn (321) diffraction peak intensity distribution across the same slice with a step size of 500 µm in horizontal and in vertical directions.

The maps in Figure 5 show the Nb_3Sn (321) and Cu (200) d-spacing variations across the coil cross section in radial and hoop direction. In order to cancel out small d-spacing errors from sample to detector distance variations, the sample was rotated by 180° after the acquisition of the first d-spacing map, and a second map was acquired. The maps acquired with the sample positions 0° and 180° were overlaid so that sample to detector distance errors are averaged out. In total 51200 XRD pattern were acquired (acquisition time 14.2 hours).

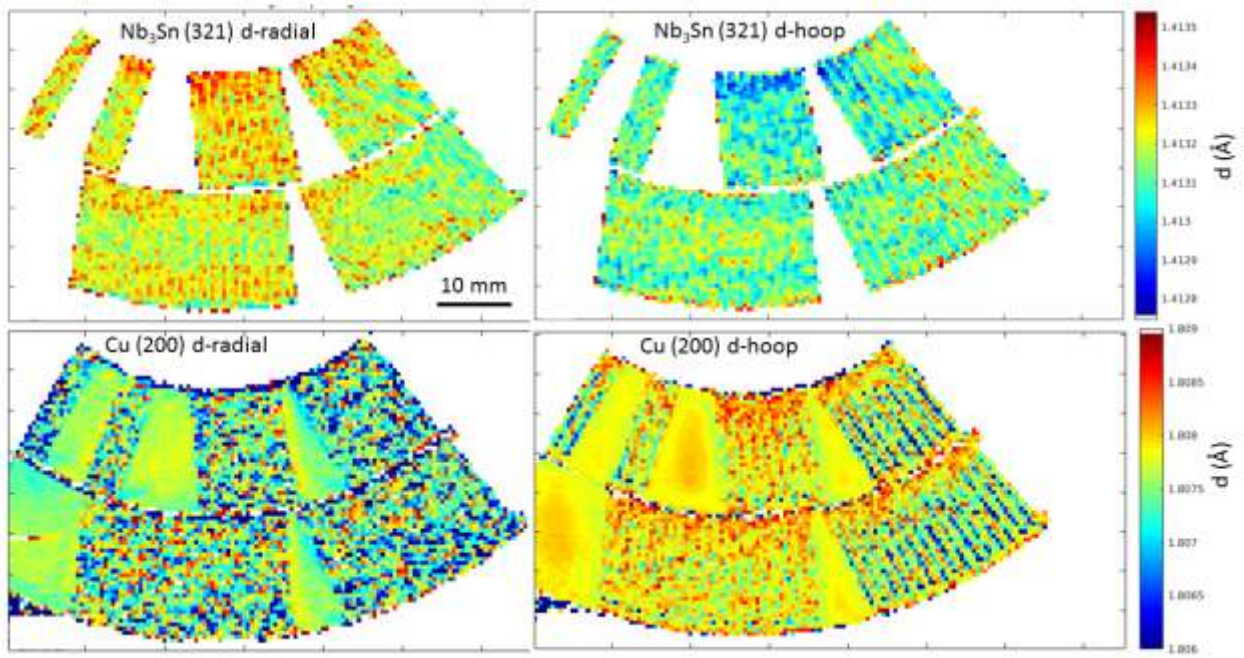

Figure 5: Nb_3Sn (321) and Cu (200) d-spacing distribution in the centre segment in radial and hoop directions.

The Nb_3Sn (321) d-spacing distribution across the coil segment from the 11 T dipole pole end is shown in Figure 6.

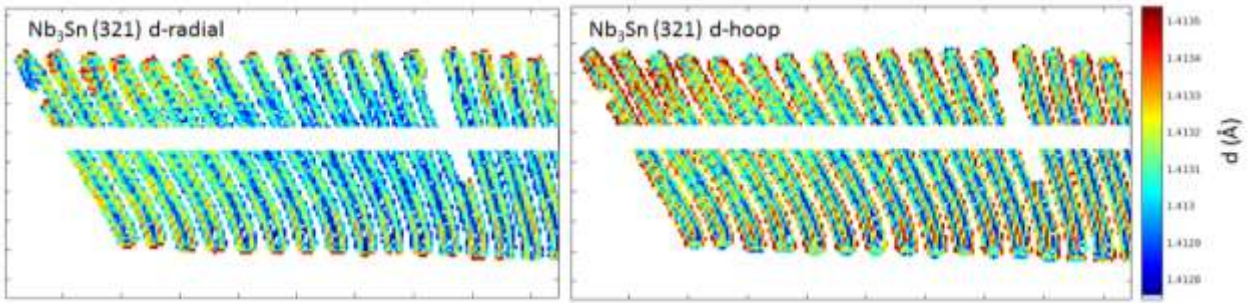

Figure 6: Nb_3Sn (321) d-spacing distribution in the pole end segment in radial and hoop directions.

In Table 2 the average Nb_3Sn (321) and Cu (200) d-spacings measured in the coil center slice and in the pole end slice are compared. The comparison with the assumed stress free Nb_3Sn (321) and Cu (200) d-spacing values (Nb_3Sn (321): d = 1.4129 Å and Cu (200): d = 1.8080 Å) indicates that Nb_3Sn is under slight axial compression of about 0.01%, and Cu under slight axial tension of about 0.02%.

The residual Nb_3Sn strain is rather homogeneous across the 11 T coil slices. In particular no strong differences between the coil center and pole end slices are observed. In the center coil segment the Nb_3Sn (321) d-spacing is in average 0.01% smaller in the hoop direction than in the radial direction, while the Cu (200) d-spacing is slightly larger in hoop direction.

Table 2: Average Nb_3Sn lattice parameters calculated from the Nb_3Sn (321) and Cu (200) d-spacings in radial and hoop directions in the different coil cross sections. The standard deviation is mainly a measure for the d-spacing variation in the analysed volume.

	Lattice parameter (Å)			
	Nb_3Sn radial	Nb_3Sn hoop	Cu radial	Cu hoop
Pole end	5.2873±0.0006	5.2877±0.0007	3.6144±0.0028	3.6146±0.0032
Coil center average	5.2877	5.2873	3.6148±0.0016	3.6156±0.0012

The Cu lattice parameters of the individual Al_2O_3 dispersion strengthened wedges are in radial direction slightly smaller than in hoop direction. The average radial and hoop lattice parameters are 3.6152±0.0001 Å and 3.6158±0.0002 Å, respectively.

In order to verify whether the spatial resolution of the diffraction experiment has an influence on the d-spacing results, an area of 3×3 mm^2 in the center of the 8 cable conductor block (Figure 7(a)) has been scanned with a step size of 100 µm (photon beam cross section was 200 µm × 200 µm). The distributions of the Nb_3Sn (321) intensity and the d-radial/d-hoop ratio are presented in Figure 7 (b) and (c), respectively. On the microscale the d-spacing pattern is clearly correlated with wire position within the coil, with lattice parameter variations of about ±0.03%. The radial/hoop d-spacing ratio is shown instead of absolute d-spacing values because the ratio is not affected by sample to detector distance uncertainties.

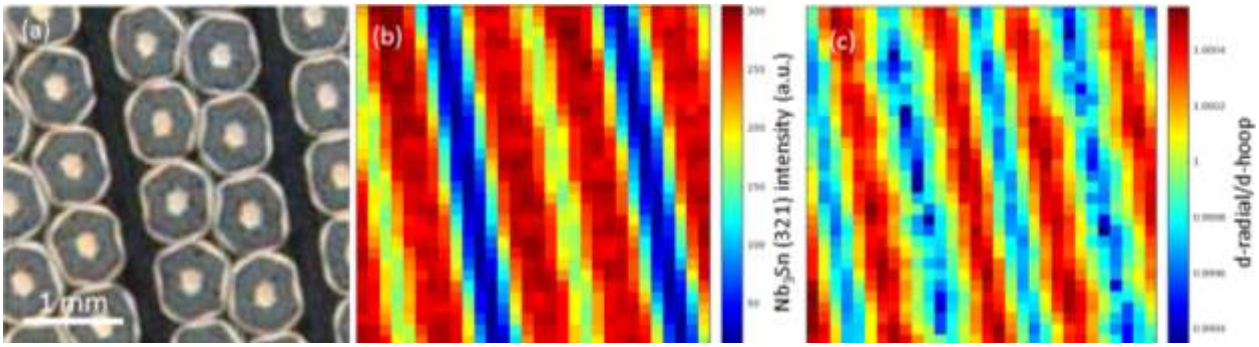

Figure 7: (a) Micrograph of the conductor block center. (b) Nb_3Sn (321) peak area and (c) radial/hoop Nb_3Sn lattice parameter acquired by high resolution scans with 100 µm step size.

3.3 Comparison of the Nb_3Sn and Cu lattice parameters in the four largest conductor blocks as determined by XRD and neutron diffraction

For the determination of the residual strain by XRD in the center of the different conductor blocks a 10 pixel × 10 pixel box filter was applied to average the d-spacing values in an area of 5 × 5mm^2. The averaged radial and hoop d-spacing values in the four largest conductor blocks are summarized in Table 3. Since the Stress-Spec instrument is measuring relative strain differences, the comparison of the radial/hoop ratio is most meaningful. It can be seen that differences in the Nb_3Sn and Cu residual strain in the different conductor blocks are small. A significantly different Nb_3Sn and Cu lattice parameter is measured in P4 in hoop direction, where the neutron diffraction reveals a compressive hoop strain that is not seen in the XRD results.

Table 3: Comparison of neutron diffraction and XRD results of Nb_3Sn and Cu lattice parameters in radial and hoop directions in the four largest conductor blocks in the 11 T coil centre. Nb_3Sn lattice parameters are calculated from the d-spacing of the (321) reflection. The Cu lattice parameter is calculated from the d-spacing of the (200) reflection (XRD) or the (220) reflection (neutron diffraction). The sample volume probed by XRD is 5×5×3 mm^3, and the neutron diffraction nominal gauge volume is 5×5×5 mm^3.

		Nb_3Sn radial	Nb_3Sn hoop	*Nb_3Sn radial/hoop*	Cu radial	Cu hoop	*Cu radial/hoop*
P1	Neutron	5.2866	5.2876	*0.9998*	3.6141	3.6157	*0.9996*
	XRD	5.2877	5.2877	*1.0000*	3.6146	3.6148	*0.9999*
P2	Neutron	5.2864	5.2871	*0.9999*	3.6141	3.6152	*0.9997*
	XRD	5.2877	5.2877	*1.0000*	3.6150	3.6156	*0.9998*
P3	Neutron	5.2869	5.2869	*1.0000*	3.6132	3.6153	*0.9994*
	XRD	5.2881	5.2873	*1.0002*	3.6148	3.6158	*0.9997*
P4	Neutron	5.2879	5.2839	*1.0008*	3.6154	3.6138	*1.0004*
	XRD	5.2877	5.2873	*1.0001*	3.6146	3.6150	*0.9999*

3.4 Residual Nb_3Sn strain in the centre of 4 conductor blocks in 4 cm-thick 11 T dipole coil segment

The residual Nb_3Sn and Cu strain in the center of the four largest conductor blocks has been determined from the axial, radial and hoop neutron diffraction measurements. Using the peak fit results of Table 4, the residual Nb_3Sn and Cu strain values have been calculated directly from the measured scattering angles according to Equation 1, relative to the assumed stress free Nb_3Sn (321) and Cu (220) angles $2\Theta_{0Nb3Sn(321)}$=72.822±0.005 and $2\Theta_{0Cu(220)}$=81.986±0.005 obtained from the extracted wire diffraction results. The possible small Cu and Nb_3Sn pre-stress in the wires is neglected in the determination of the stress free diffraction angles.

Equation 1
$$\varepsilon_{hkl} = \frac{d_{hkl} - d_{0,hkl}}{d_{0,hkl}} = \frac{\sin(\theta_{0,hkl})}{\sin(\theta_{hkl})} - 1$$

Table 4: Main Nb_3Sn (321) and Cu (220) peak fit results and calculated elastic strain in radial, hoop and axial directions at RT.

	Nb_3Sn (321)			Cu (220)		
	2Θ (°)	Int. (a.u.)	Strain (%)	2Θ (°)	Int. (a.u.)	Strain (%)
P1-radial	72.826± 0.005	10790	-0.005±0.008	82.006±0.004	74580	-0.020±0.006
P1-hoop	72.811±0.007	15000	+0.013±0.010	81.964±0.003	145200	+0.022±0.006
P1-axial	72.828±0.013	2020	-0.007±0.002	82.021±0.004	13100	-0.035±0.006
P2-radial	72.830±0.005	19270	-0.009±0.008	82.007±0.003	122640	-0.021±0.006
P2-hoop	72.819±0.011	1680	+0.004±0.001	81.976±0.003	18980	+0.010±0.006
P2-axial	72.816±0.009	7010	+0.007±0.001	81.986±0.002	22500	0.000±0.005
P3-radial	72.822±0.015	1290	0.000±0.002	82.032±0.004	13100	-0.047±0.006
P3-hoop	72.821±0.010	3130	+0.001±0.001	81.974±0.003	29390	+0.012±0.006
P3-axial	72.817±0.009	2540	+0.006±0.002	81.968±0.004	8740	+0.018±0.006
P4-radial	72.805±0.006	5610	+0.020±0.008	81.971±0.003	30680	+0.015±0.006
P4-hoop	72.870±0.007	16280	-0.056±0.010	82.014±0.003	297800	-0.028±0.006
P4-axial	72.805±0.013	2260	+0.020±0.006	81.953±0.004	7780	+0.033±0.005

The residual Nb_3Sn strain results for the different conductor blocks (P1, P2, P3 and P4 in Figure 2) are summarized in Figure 8. The error bars take into account the statistical error in the peak fit results and the estimated uncertainty of the stress free diffraction angles.

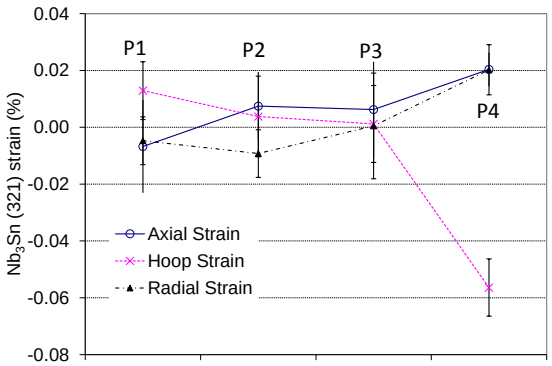

Figure 8: Residual Nb_3Sn (321) strain in axial, hoop and radial directions in the centre of the four largest conductor blocks of the 11 T coil segment.

A significant Nb_3Sn residual strain value of -0.056±0.010% is found in P4 in hoop direction. The P4 radial and axial residual Nb_3Sn strain values are 0.020±0.006% and 0.020±0.009%, respectively. Some residual strain is also revealed in the Cu stabilizer of the composite conductor.

This suggests that a plastic deformation of some coil materials has occurred during the prior magnet assembly and operation procedures. The yield strength of the annealed Cu stabilizer, as an example, is at ambient temperature only about 20 MPa [20], which is well below the expected stresses exerted on the coil.

3.5 Residual stress estimate

The corresponding residual stresses have been calculated according to Equation 2 [21,22], with the assumption that the principal stress directions are in axial, radial and hoop direction.

$$\sigma_{ii} = \frac{E_{hkl}}{1+\nu_{hkl}}\left(\varepsilon_{ii} + \frac{\nu_{hkl}}{1-2\nu_{hkl}}\left(\varepsilon_{11}+\varepsilon_{22}+\varepsilon_{33}\right)\right)$$

Equation 2

Nb_3Sn (321) elastic constants (E_{hkl}) and Poisson ratios (ν_{hkl}) have been calculated from single crystal elastic constants [23,24] using the Kröner coupling model [25] for the interaction between crystallites

(E_{Nb3Sn}=131 GPa, ν_{Nb3Sn}=0.363). The calculated residual stress values in the center of the four conductor blocks are presented in Figure 9.

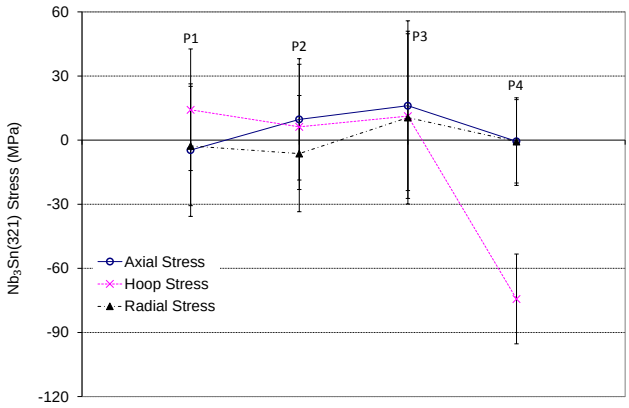

Figure 9: Residual Nb_3Sn (321) stress in axial, hoop and radial directions in the centre of the four largest 11 T dipole conductor blocks.

A significant residual compressive Nb_3Sn hoop stress of 74±21 MPa is calculated in P4. Cu residual stress is mainly detected in radial direction. Since the reflections of the strongly textured Nb could not be recorded in all directions, the mechanical stresses to which the µm-thick Nb barriers are also subjected cannot be taken into account.

3.6 Nb_3Sn and Cu lattice parameters at 7 K

Low temperature diffraction measurements were performed at Stress-Spec in radial and in hoop directions. The Nb_3Sn (321) and Cu (220) lattice parameters at 7 K and RT are compared in Table 5. In average the Nb_3Sn and Cu lattice parameters in radial and hoop directions are 0.153±0.012% and 0.334±0.008% smaller than the respective RT values. The radial Cu lattice parameter changes are slightly smaller than those in hoop direction, indicating small changes of the stress distribution during cooling down.

Table 5: Comparison between RT and 7 K Nb_3Sn (321) and Cu (220) diffraction angles.

	a-Nb_3Sn (321) (Å)			a-Cu (220) (Å)		
	RT	7 K	*Delta (%)*	RT	7 K	*Delta (%)*
P1-radial	5.2866	5.2782	*0.159*	3.6141	3.6020	*0.337*
P1-hoop	5.2876	5.2795	*0.152*	3.6157	3.6035	*0.339*
P2-radial	5.2864	5.2787	*0.145*	3.6141	3.6021	*0.332*
P2-hoop	5.2871	5.2799	*0.136*	3.6152	3.6030	*0.340*
P3-radial	5.2869	5.2791	*0.147*	3.6132	3.6015	*0.324*
P3-hoop	5.2869	5.2780	*0.169*	3.6153	3.6031	*0.338*
P4-radial	5.2879	5.2803	*0.144*	3.6154	3.6039	*0.320*
P4-hoop	5.2839	5.2750	*0.169*	3.6138	3.6014	*0.344*

The Nb_3Sn and Cu lattice parameter changes have been measured during warm up of the 11 T coil segment conductor block P1 in radial direction. Within the experimental uncertainties the lattice parameter changes are predicted by thermal expansion coefficients [26]. For comparison, the nearly stress free Nb_3Sn lattice parameter measured previously at 4.2 K in a similar RRP wire is 5.276 Å [10].

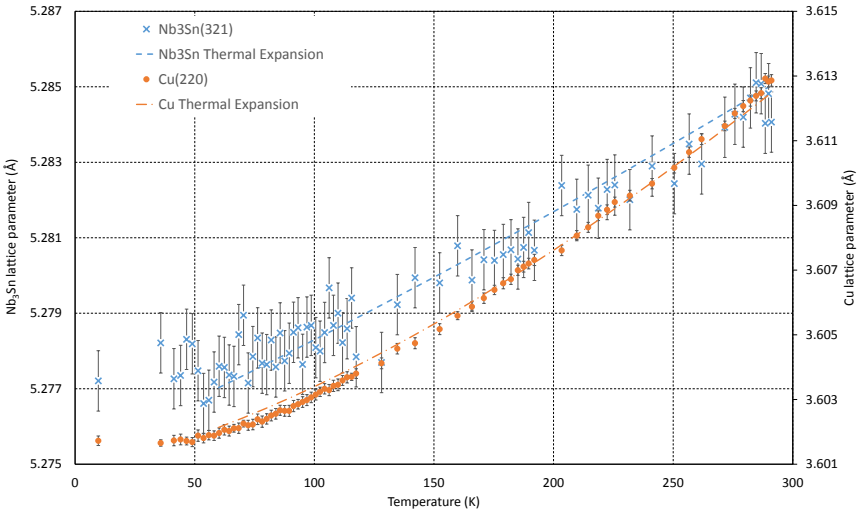

Figure 10: Nb_3Sn and Cu lattice parameter vs temperature during heating of sample coil 107-1, measurement position P1-radial.

4. Discussion

The knowledge of the Nb_3Sn strain distribution in magnet coils is required in order to predict their ultimate performance limit. So far the strain state distribution in magnet coils could only be estimated by FE simulations. Here we report for the first time direct Nb_3Sn strain distribution measurements. We have exploited the unique advantages of both high energy synchrotron XRD and complementary neutron diffraction measurements to measure the strain state in coil slices cut from the center and the pole end of an 11 T dipole coil, which was previously cold tested in a magnet. The strain state was measured at ambient temperature after removing the collars, without applied external stresses.

The very fast high energy synchrotron diffraction measurements have enabled the acquisition of Nb_3Sn strain maps with a spatial resolution of 0.5 mm across the entire coil cross section, and a 0.2 mm spatial resolution in a selected cross sectional area. Averaging XRD results acquired at sample positions 0° and 180° cancelled out sample to detector distance variations. The main drawback of the XRD measurements is the limited penetration depth, which limits the thickness of the coil segments that can be studied to about 3 mm even with 150 keV photons. Therefore, an influence of the sample preparation on the Nb_3Sn strain can probably not be excluded. The strain maps were acquired with the photon beam aligned nearly parallel to the conductor drawing direction, where strain can be measured in hoop and radial directions. Axial strain measurements are only possible in extracted wires, but not in the coil slice cross sections.

In contrast to XRD measurements, neutron diffraction measurements can probe deeply inside the Nb_3Sn coil segments. In the present case the maximum sampling depth is about 2 cm, mainly limited by the relatively strong neutron absorption in the epoxy impregnation of the coil. This enabled neutron diffraction measurements in the center of a 4 cm thick coil segment in axial, hoop and radial directions. Assuming that these are the principal stress directions, the residual strain and stress in the probed volume has been calculated.

In the present study the Nb_3Sn and pure Cu strain distribution has been analyzed. Diffraction peaks of Nb subelement barriers, of Cu-Sn bronze in the subelement centers and of the 25 µm thick steel foil in the cable have not been analyzed. Previous studies have shown that in particular the effect of the Nb barrier mechanical properties on mechanical behavior of the composite wire cannot be neglected [10].

The high spatial resolution XRD strain maps have revealed radial and hoop Nb_3Sn lattice parameter oscillations of about ±0.03%, which are correlated with wire position within the coil. Such small strains are not expected to have a strong effect on the superconducting properties. Since the Nb_3Sn subelement diameter is about 50 µm, the XRD measurements with 200 µm step size provide average lattice parameters of several

filaments. Higher spatial resolution XRD measurements using a µm size pencil beam could probe possible lattice parameter variations across individual subelements that might be caused by mechanical stresses and/or Sn concentration gradients. The lattice parameter of stress free Nb_3Sn can vary from about 5.28 to 5.29 Å, depending on the Sn content [27].

The axial Nb_3Sn pre-compression in the coil derived by XRD measurements with the beam perpendicular to the axis of extracted wires is about 0.01%. A similarly small axial Nb_3Sn pre-compression has been measured previously in the center of 10 cm long straight RRP wires [10].

The neutron diffraction results reveal a compressive Nb_3Sn hoop strain in the conductor block P4. During magnet operation this conductor block at the coil midplane is subjected to the highest stress levels, and the neutron diffraction results suggest that this causes a significant residual Nb_3Sn stress that remains after magnet disassembly and removal of the collars. This implies a plastic deformation of some coil materials, but the magnitude of the stresses that has caused this permanent deformation cannot be easily determined. In the conductor blocks P1, P2 and P3 the Nb_3Sn residual strain is smaller than the measurement uncertainties. A comparison between Nb_3Sn and Cu strain values in the different conductor blocks suggests that the Nb barriers and/or the Cu-Sn bronze subelement centers have a significant influence on the mechanical coil behavior.

During cooling to 7 K the Nb_3Sn and Cu lattice parameter changes are similar to those expected from published thermal expansion data. Slightly different Cu lattice parameter changes in the radial and hoop directions suggest that small changes of the stress distribution occur in the coil segment during cooling.

Beyond the measurement of the Nb_3Sn residual strain homogeneity in coils after the reaction heat treatment, residual strain and stress measurements as they are now possible with neutron strain scanners like Stress-Spec open the way for experiments where mechanical stress is applied for instance through steel collars as they are used in the 11 T dipole magnets. Such measurements should help to improve the understanding of the stresses exerted on the Nb_3Sn filaments during coil assembly, and to provide an experimental verification of the finite element simulation results that are the basis of the coil shimming plans.

The ultimate magnet performance limits may be estimated from superconducting wire critical current measurement results, provided that the Nb_3Sn strain state in the coil high field regions resembles that of the wire on the test barrel. Recent 11 T dipole short model magnet test results suggest that the ultimate field may be affected by the mechanical stresses at the coil mid-plane [28]. For future diffraction experiments of collared coil segments it will therefore be useful to perform diffraction measurements of the same conductor on a critical current test barrel as well.

In situ experiments for measuring the Nb_3Sn strain state under varying applied load are possible too. In order to define the coil segment size and shape suitable for such experiments, the time needed for the acquisition of diffractograms with acceptably small statistical error, as well as the maximum forces of the available load frames need to be considered. Direct Nb_3Sn elastic strain measurements at cryogenic temperature under applied load are particularly challenging and would probably require the development of a dedicated test set-up.

Assuming that axial, hoop and radial are the principal stress directions residual stress can be calculated from the strain results in these directions. If the principal stress directions are not known, diffraction measurements in at least 6 orientations are needed. For the residual stress calculations the hkl elastic constants need to be known, and the Nb_3Sn texturing needs to be considered as well [29].

5. Conclusion

At room temperature in the RRP conductor in the 11 T dipole coil Nb_3Sn is at RT under slight axial compression of about 0.01%, and Cu under slight axial tension of about 0.02%.

In the 11 T dipole center coil segment the Nb_3Sn (321) d-spacing is in average 0.01% smaller in the hoop direction than in the radial direction, while the Cu (200) d-spacing is slightly larger in hoop direction.

On the microscale the Nb_3Sn d-spacing pattern is clearly correlated with the wire position within the coil, with hoop and radial lattice parameters oscillating by about ±0.03%.

Overall XRD and neutron diffraction results are in reasonable agreement. A significantly different Nb_3Sn and Cu lattice parameter is measured in the center of conductor block at the coil mid-plane (P4) in hoop direction, where the neutron diffraction reveals a compressive residual strain of 0.056±0.010%. In the conductor blocks P1, P2 and P3 the Nb_3Sn residual strain values are smaller than the statistical uncertainty in the neutron diffraction results.

Acknowledgments

This work was supported by the European Commission under the FP7 project HiLumi LHC under Grant GA 284404, co-funded by the DoE, USA and KEK, Japan.

Part of this work is based upon experiments performed at the Stress-Spec instrument operated by FRM II at the Heinz Maier-Leibnitz Zentrum (MLZ), Garching, Germany.

References

1 L. Bottura, G. de Rijk, L. Rossi, E. Todesco, "Advanced accelerator magnets for upgrading the LHC," IEEE Trans. Appl. Supercond., 22(3), (2012). 4002008

2 The High Luminosity Large Hadron Collider, ed. O. Bruening and L. Rossi, World Scientific Publishing Co, (2015)

3 J.W. Ekin, "Strain scaling law for the flux pinning in practical superconductors. Part 1: basic relationship and application to Nb_3Sn conductors" Cryogenics 20 (1980), 611

4 R. Flükiger, W. Schauer, W. Specking, L. Oddi, L. Pintschovius, W. Müllner, B. Lachal, "The Phase Relationships in Nb_3Sn Wires at Low Temperatures as Detected by Crystallographical (Neutron and X-ray Diffraction) and by Physical [Bc2(T), Jc vs. ε] Measurements", Adv. Cryo. Engrg. Materials, 28, 361 (1982)

5 B. ten Haken, A. Godeke, H.H.J. ten Kate, IEEE Trans. Magn. 5, (1995), 1909–12

6 C. Sanabria, P.J. Lee, W. Starch, I. Pong, A. Vostner, M.C. Jewell, A. Devred, D.C. Larbalestier, "Evidence that filament fracture occurs in an ITER toroidal field conductor after cyclic Lorentz force loading in SULTAN", Supercond. Sci. Technol. 25 (2012), 075007

7 W. Goldacker and R. Flükiger, "Direct observation of crystallographical changes at 10 K caused by the application of varying stresses to Nb_3Sn wires," Journal de Physique, vol. 45, pp. 387-390, 1984.

8 B. ten Haken, A. Godeke, and H. H. J. ten Kate, "Investigation of microscopic strain by X-ray diffraction in Nb3Sn tape conductors subjected to compressive and tensile strains," Adv. Cryo. Eng., vol. 42, pp. 1463-1470, 1996.

9 C. Scheuerlein, M. Di Michiel, F. Buta, "Synchrotron radiation techniques for the characterisation of Nb_3Sn superconductors", IEEE Trans. Appl. Supercond. 19(3), (2009), 2653-2656

10 C. Scheuerlein, M. Di Michiel, F. Buta, B. Seeber, C. Senatore, R. Flükiger, T. Siegrist, T. Besara, J. Kadar, B. Bordini, A. Ballarino, L. Bottura, "Stress distribution and lattice distortions in Nb_3Sn/Cu multifilament wires under uniaxial tensile loading at 4.2 K", Supercond. Sci. Technol. 27, (2014), 044021

11 C. Scheuerlein, U. Stuhr, L. Thilly, "In-situ neutron diffraction under tensile loading of powder-in-tube Cu/Nb_3Sn composite wires: effect of reaction heat treatment on texture, internal stress state and load transfer", Appl. Phys. Lett., 91(4), 042503, (2007)

12 T Hemmi, S Harjo, Y Nunoya, H Kajitani, N Koizumi, K Aizawa, S Machiya and K Osamura, "Neutron diffraction measurement of internal strain in the first Japanese ITER CS conductor sample", Supercond. Sci. Technol. 26 (2013) 084002 (6pp)

13 M. Karppinen et al., "Design of 11 T twin-aperture dipole demonstrator magnet for LHC upgrades", IEEE Trans. App. Supercond., vol. 22, no. 3, June 2012

14 E. Barzi, N. Andreev, M. Karppinen, V. Lombardo, F. Nobrega, D. Turrioni, R. Yamada, A.V. Zlobin, "Development and fabrication of Nb_3Sn Rutherford cable for the 11 T DS dipole demonstration model," IEEE Trans. Appl. Supercond., 22(3), (2012), 6000805

15 U. Kelly, S. Richter, C. Redenbach, K. Schladitz, C. Scheuerlein, F. Wolf, P. Ebermann, F. Lackner, D. Schoerling, D. Meinel, "3D shape and cross sectional inhomogeneity of Nb_3Sn superconducting wires in Rutherford cables",IEEE Trans. Appl. Supercond., submitted

16 J. A. Parrell, M. B. Field, Y. Zhang, and S. Hong, Adv. Cryo. Eng. (Materials) 50B, 369 (2004).

17 T. Koettig, W. Maciocha, S. Bermudez, J. Rysti, S. Tavares, F. Cacherat, J. Bremer, “Thermal conductivity measurements of impregnated Nb3Sn coil samples in the temperature range of 3.5 K to 100 K”, IOP Conf. Series: Materials Science and Engineering 171 (2017) 012103

18 C. Scheuerlein, G. Arnau, P. Alknes, N. Jimenez, B. Bordini, A. Ballarino, M. Di Michiel, L. Thilly, T. Besara, T. Siegrist, “Nb_3Sn texture in state-of-the-art multifilamentary superconducting wires”, Supercond. Sci. Technol., 27, (2014), 025013

19 M. Hofmann, R. Schneider, G.A. Seidl, J. Rebelo-Kornmeier, R.C. Wimpory, U. Garbe, H.-G. Brokmeier, “The new materials science diffractometer STRESS-SPEC at FRM-II, Physica B 385-386 (2006) 1035-1037

20 C. Scheuerlein, F. Lackner, F. Savary, B. Rehmer, M. Finn, P. Uhlemann, “Mechanical properties of the HL-LHC 11 Tesla Nb3Sn magnet constituent materials”, IEEE Trans. Appl. Supercond., 27(4), (2017), 4003007

21 M. T. Hutchings, P. J. Withers, T. M. Holden and T. Lorentzen, “Introduction to the Characterization of Residual Stress by Neutron Diffraction”, 2005, Boca Raton, FL, CRC Taylor & Francis

22 R.A. Winholtz, A.D. Krawitz, “The effect of assuming the principal directions in neutron diffraction measurement of stress tensors”, Materials Science and Engineering A205 (1996) 257-258

23 K.R. Keller, J.J. Hanak, “Lattice softening in single crystal Nb_3Sn”, Phys. Lett., vol. 21(3), (1966), 263-264,

24 H. Wern, R. Johannes, H. Walz, "Dependence of the X-Ray Elastic Constants on the Diffraction Plane", phys. stat. sol. (b) 206(2), (1998), 545-557

25 E. Kröner, “Berechnung der elastischen Konstanten des Vielkristalls aus den Konstanten des Einkristalls“, Zeitschrift für Physik, 151(4), (1958), 504–18

26 N. Mitchell, “Finite element simulations of elasto-plastic processes in Nb_3Sn strands”, Cryogenics 45 (2005) 501-505

27 H. Devantay, J. L. Jorda, M. Decroux, J. Müller and R. Flükiger, J. Mater. Sci. 16, 2145 (1981)

28 G. Willering, M. Bajko, H. Bajas, B. Bordini, L. Bottura, J. Feuvrier, L. Fiscarelli, S. Izquierdo Bermudez, C. Löffler, F. Mangiarotti, E. Nilsson, J-C. Perez, G. de Rijk, F. Savary, “Comparison of Cold Powering Performance of 2-m long Nb3Sn 11T Model Magnets”, IEEE Trans. Appl. Supercond., submitted

29 C. Scheuerlein, B. Fedelich, P. Alknes, G. Arnau, R. Bjoerstad, B. Bordini, “Elastic anisotropy in multifilament Nb_3Sn superconducting wires”, IEEE Trans. Appl. Supercond., 25(3), (2015), 8400605